Journal Name

Dynamic Article Links ▶

ARTICLE TYPE

Preparation of magnetic core-shell nanoflowers Fe₃O₄@MnO₂ as reusable oxidase mimetics for colorimetric detection of phenol

Yuhao Xiong, Siheng Chen, Fanggui Ye*, Linjing Su, Cong Zhang, Shufen Shen, Shulin Zhao

In this paper, magnetic core-shell nanoflowers Fe₃O₄@MnO₂ were fabricated via a solvothermal method. We demonstrated that the as-synthesized magnetic nanoflowers Fe₃O₄@MnO₂ possess intrinsic oxidase-like activity in a wide range of pH and can catalytically oxidize substrate 4-aminoantipyrine (4-AAP) and phenol to form pink color products without the requirement for additional oxidizing agents. On 10 the basis of this phenomenon, a simple colorimetric method for the determination of phenol was developed. A wide linear detection range can be obtained from 1.0 μM to 120 μM (R^2= 0.9962) with a detection limit of 0.15 μM. And the method was applied to determination of phenol in wastewater with good recoveries ranging from 96.0 to 101.5%. Furthermore, benefited from chemical stability and easily of recycle (by simple magnetic separation) of Fe₃O₄@MnO₂, the oxidase mimetics own excellent 15 reusability and reproducibility in cycle analysis.

1. Introduction

Phenols are common environmental pollutants generated from industrial and agricultural processes, such as petroleum refining, pesticide, and plastics. Despite their commercial importance, but 20 phenols are considered not only toxic chemicals, but also highly hazardous materials. This is due to the fact that they can be easily absorbed by animals and humans, through the skin and mucous membrane[1]. For their damage to natural environment and potential threat to human health, phenols have been listed as the 25 priority control pollutants by US Environmental Protection Agency[2]. Thus, it is essential to develop sensitive, selective and reliable analytical methods for determination of phenols in water.

Up to now, chromatography[3-5], electrochemical[6-9], chemiluminescence[10, 11] and spectrophotometry[12, 13], are the most 30 widely used analytical methods for analysis of phenols. Though most of these methods yield high sensitivity and high reproducibility, they usually require to expensive instruments, extensive purification, which limit their wide application. Colorimetric biosensing has drawn intense attention in biological 35 science and analytical chemistry due to the potential for direct visual readout. It has advantages of simplicity, rapidity, and cheapness as well as the fact that there is no requirement for any sophisticated instrumentation. Since Emerson and Ettinger's pioneering work on the K₃Fe(CN)₆-based chromogenic reaction 40 for measurement of phenolic compounds[14, 15], a great deal of excellent works about the novel materials for chromogenic detection of phenolic compounds have been done[16-21]. Recently, Zare's[22] and Lin's[23] groups reported using enzyme-inorganic hybrid nanoflowers as catalyst for visual detection of aqueous 45 phenol solutions, respectively. Aston et al. reported ultrafine composite fibers of silicate-polymer matrix structure incorporating tyrosinase enzyme for phenol detection[24]. Although enzyme-based hybrid materials are certainly attractive for colorimetric detection of phenol, the immobilized enzymes 50 activity is hampered by environmental changes, such as temperature, solution acidity and inhibitors. Also, they are limited source, costly to purify and can be difficult to store. Enzyme-mimetic inorganic nanomaterials could improve properties relative to enzyme-based hybrid materials, such as greater 55 resistance to extremes of pH and temperature and lower sensitivity to proteases[25, 26]. Previously, Rajendiran and Santhanalakshmi found that some water-soluble metal tetrasulfophthalocyanine complexes could catalyze the chromogenic reaction between phenol and 4-aminoantipyrine (4-60 AAP) assisted with H₂O₂[27]. Rezzano's group reported that Au/porphyrin composite could catalyze H₂O₂ oxidation of phenols substrates in the presence of 4-AAP in aqueous solution[20]. Gong's[18] and Li's[28] groups presented that phenolic compounds could be oxidized rapidly and transformed into pink dyes in the 65 presence of 4-AAP and phthalocyanine complexes and tert-butylhydroperoxide (t-BuOOH)[18, 28]. However, these colorimetric methods usually require additional oxidant (such as corrosive H₂O₂ or toxic t-BuOOH).

To settle the above problem, Yan et al.[29] presented that 70 tetranitro iron (II) phthalocyanine have an enzyme mimetic activity, and catalyze the substrate phenolic pollutant assisted with 4-AAP. Ding et al.[19] reported using 4-AAP chromogenic identification of chlorophenol pollutants by manganese phthalocyanine under sunlight irradiation. However, this kind of 75 catalyst can be used only once, it is hard to recycle and apt to cause secondary environmental pollution. Therefore, the exploration of novel enzyme-mimetics for catalytic oxidation of phenolic compounds for colorimetric detection remains an active

topic.

In recent years, manganese dioxides (MnO_2) have drawn particular attention due to their low cost, high activity, and non-toxicity[30-33]. Base on its high catalytic activity, bovine serum albumin-stabilized MnO_2 nanoparticles had been used for colorimetric detection[34, 35]. Unfortunately, the separation of pure nanosized MnO_2 from heterogeneous systems is one remaining technical bottleneck that hampers its wide application[36]. Thus, the development of reusable and stable magnetic MnO_2 for colorimetric detection is highly desirable.

In this work, a new reusable magnetic core-shell nanoflower like enzyme-mimetic $Fe_3O_4@MnO_2$ was fabricated and characterized in detail. Then, the prepared $Fe_3O_4@MnO_2$ was first functioned as a reusable efficient catalyst and successfully used for the simple, selective colorimetric determination of phenol. The possible mechanism involved chromogenic detection was also proposed. Further studies demonstrated that the as-prepared $Fe_3O_4@MnO_2$ exhibits good recycled, high stability and high catalytic activity in aqueous solution.

2. Experimental

2.1 Chemicals and reagents

All chemicals were at least of analytical grade. Ferric chloride hexahydrate ($FeCl_3 \cdot 6H_2O$) was purchased from Aladdin (Shanghai, China). Ethylene glycol, sodium acetate (NaAc), potassium permanganate ($KMnO_4$), potassium dichromate ($K_2Cr_2O_7$), iso-propanol, hydrochloric acid （HCl）, 4-aminoantipyrine (4-AAP) were purchased from Shantou Xilong Chemical Factory (Guangdong, China). Polyethylene glycol 6000 (PEG 6000) was obtained from J&K Chemical Technology (Beijing, China). Ultrapure water (18.2 MΩ cm) was produced by a Millipore purification system (Bedford, MA, USA) and used to prepare all aqueous solutions.

2.2 Preparation of Fe_3O_4 magnetic nanoparticles

Magnetic Fe_3O_4 nanoparticles were synthesized according to the previous work.[37] Briefly, 1.35 g of $FeCl_3 \cdot 6H_2O$ was added to 40 mL of ethylene glycol to form a clear solution and then 3.6 g of NaAc and 1.0 g of PEG 6000 were added. The mixture was stirred vigorously for 30 min and then sealed in a 50 mL Teflon-lined stainless-steel autoclave. The autoclave was then placed in an oven at 200℃ for 8 h. After the mixture was naturally cooled, the black products were thoroughly washed with ethanol and vacuum dried at 60 °C.

2.3 Preparation of core-shell $Fe_3O_4@MnO_2$ magnetic nanocomposites

The $Fe_3O_4@MnO_2$ was synthesized according to literatures with some modifications.[38] In particular, 0.5 g of $KMnO_4$ was dissolved in 35 mL of ultrapure water with vigorous stirring, followed by 0.7 mL of HCl (37 wt %) was then slowly added dropwise. The solution was stirred continuously for 10 min, and then 0.3 g of Fe_3O_4 magnetic nanoparticles was added and transferred into a 50 mL teflon-lined stainless-steel autoclave, which was heated at 110°C for a period of 6 h in an electric oven. The obtained products were washed several times with ultrapure water and ethanol, and finally dried under vacuum at 60℃ for 12 h.

2.4 Instrumentation

Absorption spectra were recorded on a model Cary 60 spectrophotometer (Agilent, USA). Fourier transform infrared (FT-IR) (4000-400 cm^{-1}) in KBr were recorded using a PE Spectrum One FT-IR spectrometer (PE, USA). Transmission electron microscopy (TEM) images were captured using a Tecnai G2 T20 electron microscope (FEI, USA). The scanning electron microscopy (SEM) images were taken by a SU8020 field-emission scanning electron microscope (Hitachi, Japan). The magnetization curves were measured at 300 K under a magnetic field (in the range of −20 and 20 kOe) on a MPMS-XL-7 magnetometer (Quantum Design, USA).

2.5 Detection of phenol

In a typical process, 5.0 mg of $Fe_3O_4@MnO_2$ was dispersed in 1.9 mL of different concentration of phenol solution. Then, 100 μL of 4-AAP solution (2.5 mg/mL) was added. After incubated at room temperature for 20 min, the reaction solution was separated immediately by a magnetic field, and the absorbance of the supernatant was measured at the calibrated maximum wavelength (λ_{max}) of 505 nm.

2.5 Calculation of detection limit

Limit of detection (LOD) is an important indicator to estimate the sensitivity of analysis methods. Here, IUPAC recommended methodology that utilized an experimentally determined signal-to-noise ratio (S/N) was employed to obtain LOD[39]. The absorbance at 505 nm of the sample containing 4-AAP and without phenol as a control was measured 20 times. Average absorbance intensity (average $_{blank}$) along with the associated standard deviation (SD $_{blank}$) was calculated on the basis of the above data, and the obtained SD $_{blank}$ was regarded as the noise (N). Then, the absorbance intensity of adding standard phenol solution with a relatively low concentration were measured for five times, and the average value (average $_{sample}$) was calculated. Finally, S/N was calculated as follow:

$$S/N = \frac{(\text{average}_{sample} - \text{average}_{blank})}{SD_{blank}}$$

Hence, a sample concentration that meets the condition of $3 < S/N < 5$ was defined as LOD.

3. Results and discussions

3.1 Characterization of the $Fe_3O_4@MnO_2$

To gain a better understanding of the morphology of the as-synthesized samples, the $Fe_3O_4@MnO_2$ was characterized by SEM and TEM (Fig.1). SEM investigations revealed that the prepared sample is uniform in all observation fields and presents nanostructures with flower-shaped morphologies. And the TEM image showed the finally formed $Fe_3O_4@MnO_2$ magnetic microspheres are composed of a Fe_3O_4 core and a MnO_2 shell, clearly demonstrating the formation of a core–shell structure. The saturation magnetization value of $Fe_3O_4@MnO_2$ was 32 emu/g (Fig.2), which was sufficient to accomplish fast and efficient
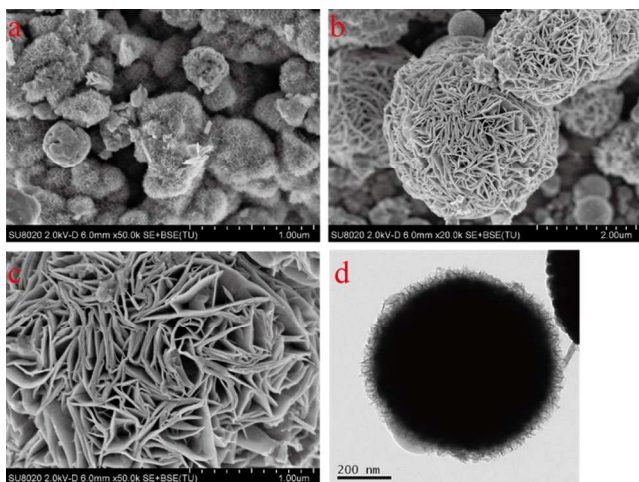
Fig. 1 The SEM (a-c) and TEM (d) images of the $Fe_3O_4@MnO_2$

Fig. 3 FT-IR spectra of $Fe_3O_4@MnO_2$

separation with an external magnetic field. This excellent magnetic responsiveness will contribute greatly to reclamation
5 and recycling. To further confirm the formation of $Fe_3O_4@$ MnO_2, FT-IR analysis was conducted to reveal the surface nature of $Fe_3O_4@$ MnO_2 (Fig.3). Absorption peaks appearing at 3407 cm^{-1} is associated with vibrations OH of the absorbed water molecules. The observed bands at 1627 and 1387 cm^{-1} correspond
10 to the symmetric C−O stretching and the asymmetric stretching of COO−, respectively. The peak at 575 cm^{-1} corresponds to the Fe−O stretching vibrations in iron oxide. In addition, the peaks at about 459, 505 and 533 cm^{-1} are related to Mn–O from the structure of MnO_2[40].

15 **3.2 Chromogenic reaction and proposed mechanism of phenol catalyzed by $Fe_3O_4@MnO_2$**

As shown in Fig.4, in the presence of $Fe_3O_4@MnO_2$, only phenol or 4-AAP solution displayed a negligible absorption in 505 nm, indicating that no oxidation reaction occurred. In the
20 absence of $Fe_3O_4@MnO_2$, the mixture of phenol and 4-AAP solution lack of obvious absorption. In contrast, addition of $Fe_3O_4@MnO_2$ produced a typical pink color in the phenol and 4-AAP solution mixture, and the pink solution exhibited intense characteristic absorbance at 505 nm.
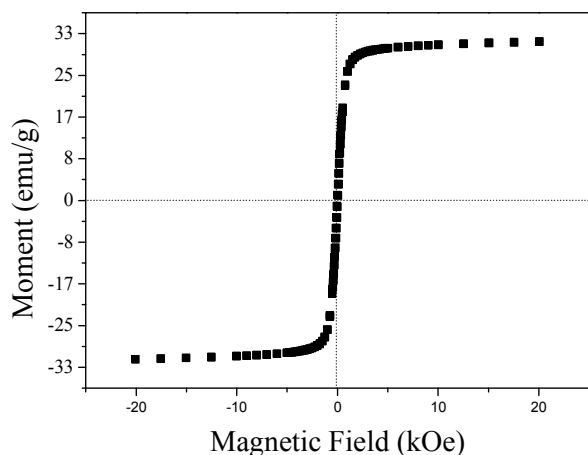
In the reaction system, no oxidants were employed, so we
30 hypothesize that the dissolved O_2 was the possible oxidant. In order to investigate whether the dissolved O_2 in the solution played a role on the catalytic oxidation, two sets of experiments were conducted: the first one was performed in the presence of O_2, the other contrast experiment was performed with continuous
35 nitrogen-bubbling to eliminate the dissolved O_2 in solution before the reaction. As the photograph shown in Fig.5a, they exhibited almost the same pink color, the absorbance of the nitrogen-bubbling was 1.24 and the other was 1.25 at 505 nm. This indicated that the O_2 in the solution had little effect on the
40 reaction. This phenomenon makes us confused, to further confirm whether the adsorption O_2 in $Fe_3O_4@MnO_2$ is the possible oxidant, the $Fe_3O_4@MnO_2$ without degassing and $Fe_3O_4@MnO_2$ degassed by five times nitrogen-pump-nitrogen cycles were used to catalyze the nitrogen-bubbling phenol and 4-AAP mixed
45 solution. As the photograph shown in Fig.4b, both of them produced pink colors, but the color of $Fe_3O_4@MnO_2$ without degassing is much darker than $Fe_3O_4@MnO_2$ degassed by five times nitrogen-pump-nitrogen, the absorbance of $Fe_3O_4@MnO_2$ degassed and without degassing were 0.75 and 1.56 respectively.
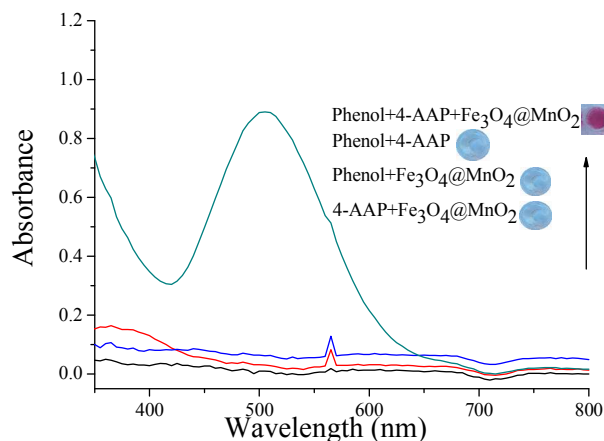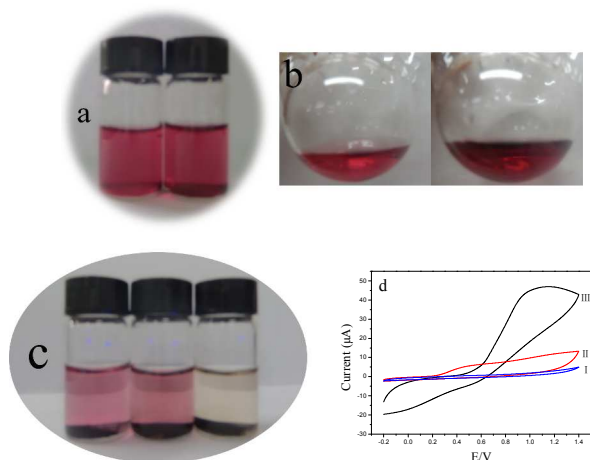50 It is suggested that adsorption O_2 was crucial for the oxidation of

25

Fig. 2 The magnetic hysteresis loops of $Fe_3O_4@MnO_2$

**Fig. 4** UV-vis spectra of phenol/4-AAP reaction solutions catalytically oxidized by the $Fe_3O_4@MnO_2$

Fig. 5 Photographs of phenol/4-AAP solutions in the absence and presence of an O₂ oxidation reaction catalyzed by Fe₃O₄@MnO₂ (a)
5 Photographs of phenol/4-AAP solution oxidation reaction catalyzed by Fe₃O₄@MnO₂ without degassing and degassed by five nitrogen−pump−nitrogen cycles (b) Photographs of the oxidation color reaction phenol/4-AAP, phenol/4-AAP/iso-propanol and phenol/4-AAP/K₂Cr₂O₇ (From left to right) (c) Cyclic voltammograms of bare GCE (Ⅰ),
10 the Fe₃O₄ modified GCE (Ⅱ) and Fe₃O₄@MnO₂ modified GCE (Ⅲ) in a 0.1 M acetic acid−acetate buffer (pH 6.0)+ phenol/4-AAP solution (d)

phenol. After degassing Fe₃O₄@MnO₂ still show catalytic ability, shown the O₂ on the surface of Fe₃O₄@MnO₂ was not only physical adsorption, but also chemisorbed O₂ probably existed on
15 the surface of Fe₃O₄@MnO₂ because of larger surface energy of nanomaterials caused by the high specific surface area[41].

Generally speaking, active oxygen radicals such as $O_2^{\bullet-}$ and $OH^{\bullet}$ obtained from O₂ molecule trap electron could initiate oxidation reaction. To further confirm the existence of specific reactive
20 species, two scavengers (iso-propanol for $OH^{\bullet}$, K₂Cr₂O₇ for $O_2^{\bullet-}$) were employed. When iso-propanol was introduced into the reaction solution, there was almost no influence on the formation of pink dye, which suggested that the formation of pink dye was not mediated by $OH^{\bullet}$ radicals. On the contrary, when iso-
25 propanol was replaced by K₂Cr₂O₇, the generation of pink dye was obviously suppressed (Fig.5c), indicating that $O_2^{\bullet-}$ was the major active species.

As we know that intense electron transfer is advantageous to produce active oxygen radicals ($O_2^{\bullet-}$). For this reason, the
30 electrocatalytic behavior of a Fe₃O₄@MnO₂ modified glassy carbon electrode (GCE) toward the electrochemical oxidation of phenol and 4-AAP were studied using cyclic voltammetry (CV). The CVs of phenol and 4-AAP at a bare GCE, Fe₃O₄ modified GCE and the Fe₃O₄@MnO₂ modified GCE are shown in Fig.5d.
35 The increased current was obviously observed under the Fe₃O₄@MnO₂ modified GCE, suggesting that the Fe₃O₄@MnO₂ had the ability to accelerate the electron transfer.

Taken together, the proposed mechanism for chromogenic of phenol substrates could be explained as following process: First,
40 successive single electron transfer from the donor of hydroxyl oxygen of phenol to the acceptor of adsorption O₂ in Fe₃O₄@MnO₂, this reactions generated the quinoid radical and $O_2^{\bullet-}$ (Fig.6a). Then, the active $O_2^{\bullet-}$ could react with 4-AAP to form the antipyrine-NH$^{\bullet}$ (Fig.6b). Finally, the generated quinoid
45 radical and antipyrine-NH$^{\bullet}$ would undergo the oxidative coupling
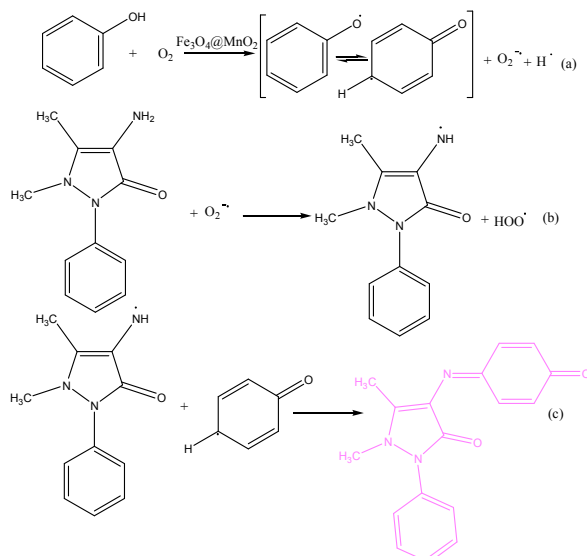
**Fig. 6** Proposed mechanism of phenol catalyzed by Fe₃O₄@MnO₂

reaction to produce the final pink color antipyrilquinoneimine (Fig.6c)[29].

50 **3.3 Optimization of detection conditions**

In order to obtain the best performance of our colorimetric method, the reaction conditions were evaluated (Fig.7a-7d).
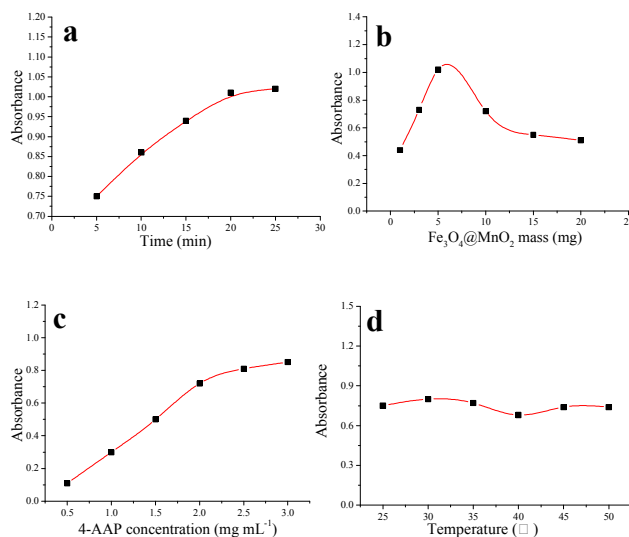
55 **Fig. 7** Effects of incubation time (a), dosage of the Fe₃O₄@MnO₂ (b), 4-AAP concentration (c), temperature (d)
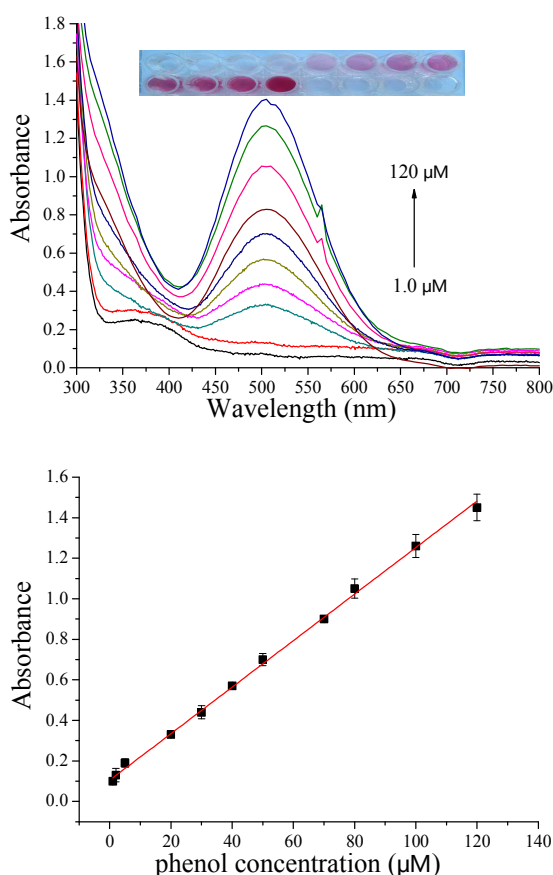
Fig. 8 Typical UV-Vis spectra, photograph and linear calibration of reaction system at varied phenol concentrations

Generally, catalytic reaction takes some time to reach equilibrium. The effect of the incubation time between 4-AAP and phenol on the formation of the pink antipyrilquinoneimine was investigated. As shown in Fig.7a, the absorbance signal firstly increased with increasing the incubation time and tended to reach a maximum value at 20 min. A further increase of the incubation time did not obviously improve the absorbance. Hence, an incubation time of 20 min was selected in the subsequent work. As we know that the dosage of catalyst plays an important role in catalytic reaction, so the effect of different amounts of $Fe_3O_4@MnO_2$ was investigated. As indicate in Fig.7b, absorbance intensity of the system increase gradually with increasing the amount of $Fe_3O_4@MnO_2$. However, if the $Fe_3O_4@MnO_2$ continues to increase, the absorbance intensity would decrease. This may be the excess $Fe_3O_4@MnO_2$ plays a role of adsorbent for the pink antipyrilquinoneimine adsorption, thus leading to a fall in absorbance. So we employed 5.0 mg as the amount of $Fe_3O_4@MnO_2$. Moreover, the optimum 4-AAP concentration has been investigated to be 2.5 mg/mL (Fig.7c). In addition, incubation temperature we also investigated. As seen in Fig.7d, the temperature effect on reaction system is very slight and negligible. Hence, room temperature (25 ℃) was selected. The exprimental result shows the tiny fluctuations of absorbance in the pH range from 5.0 to 9.0, indicating the $Fe_3O_4@MnO_2$ could work in broad pH value (data not shown). Hence, pH=7.0 was selected in the subsequent work.

3.4 Validation of the method

Under the optimal conditions, we explored the absorbance at 505 nm in the presence of different concentrations of phenol. The UV-vis spectra, typical photographs and calibration graph are shown in Fig.8. The calibration graph of the absorbance versus phenol concentration was linear in the range from 1.0 to 120 μM, the regression equation is Y=0.011X+0.11, R^2=0.9962, where Y is the absorbance intensity at 505 nm and X is the concentration of phenol. The LOD for phenol calculated to be 0.15 μM. These results indicated that this method could be used to detect the content of phenol compounds.

### 3.5 The effect of coexisting substances

To test the specificity of this analytical strategy, control experiments were carried out using phenylamine, toluene, ethanol, acetone, and so on. The concentrations of these control molecules were all 50 times compared to phenol. As shown in Fig.9, although the concentration of coexisting substances were 50-fold higher than that of phenol, the absorbance obtained for control molecules were still weak, the color differences could be judged by naked eye. This illustrates that the coexisting substances did not interfere with the determination of phenol. Therefore, the present colorimetric method showed high sensitivity and selectivity towards phenol.

3.6 Determination of phenol in real samples

The proposed method was applied to analyze wastewater samples obtained from sewage treatment plant (Guilin China). The results are listed in Table1. The recoveries of the two samples ranged from 96.0 to 101.5%, the RSDs were achieved in the range of 1.1−4.7% (n=3). All the characteristic parameters of the method validated that this simple method was reliable and sensitive for the visual detection of phenol compounds in water.

3.7 Reusability and reproducibility

For an excellent catalyst, the reusability is essential and the re-usability test of the $Fe_3O_4@MnO_2$ nanoflowers was investigated by conducting the experiment independently for 10 times. Each
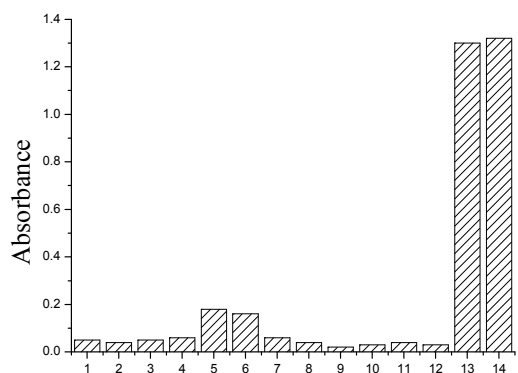
Fig. 9 Determination of the selectivity of phenol detection (from left to right: 1, aniline；2,toluene；3, ethanol；4, acetone；5, benzoic acid；6, cyclohexanol；7, imidazole；8, sodium laurylsulfonate；9,sodium sulfate；10, potassium carbonate；11, cupric acetate；12, ferric chloride；13, phenol；14, mixed sample)

ARTICLE TYPE

Table1. Results for the determination of the phenol in two wastewater samples

Sample	Original amount (µM)	Added (µM)	Found (µM)	Recovery (%)	RSD (%)
		5.0	4.9	98.0	4.7
Sample 1	N.D.[a]	20.0	20.3	101.5	2.6
		50.0	48.2	96.4	1.1
		5.0	4.8	96.0	4.3
Sample 2	N.D.	20.0	19.9	99.5	2.1
		50.0	50.1	100.2	1.3

[a]N.D., not detected

time after analysis, the $Fe_3O_4@MnO_2$ nanoflowers were separated by using a permanent magnet and washed with ethanol 5 and water respectively, and then subjected to the next run. Fig.10 presents the cycle performance of $Fe_3O_4@MnO_2$ nanoflowers, the results reveal that no loss of activity was observed even after 10 cycles, indicating the extraordinary stability of $Fe_3O_4@MnO_2$ and their excellent reproducibility.

10 Conclusions

In summary, excellent reusable magnetic core-shell $Fe_3O_4@MnO_2$ nanoflowers were fabricated and demonstrated that $Fe_3O_4@MnO_2$ could efficiently catalyze the adsorption O_2 existed on the surface of $Fe_3O_4@MnO_2$ oxidation of phenol 15 substrates assisted with 4-AAP for colorimetric determination of phenol in water. Experiments testified that the generation of $O_2^{\bullet-}$ is the key role for initial phenol oxidation and subsequent
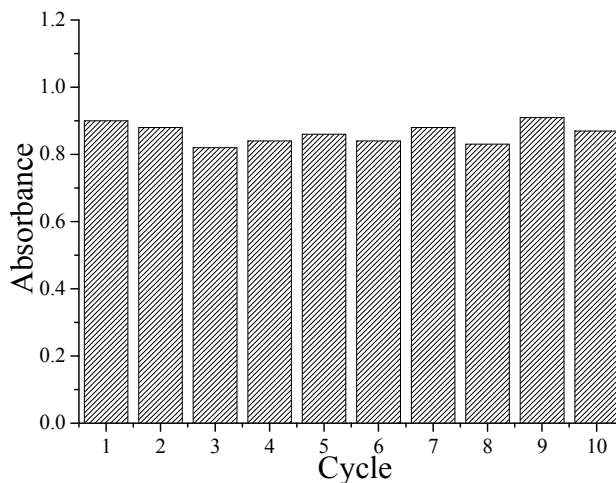
Fig. 10 Ten consecutive catalysis cycles of $Fe_3O_4@MnO_2$

20 formation pink antipyrilquinoneimine. Additionally, $Fe_3O_4@MnO_2$ owned long-term stability (no activity loss after 10 cycles) and ease of recovery (by simple magnetic separation).
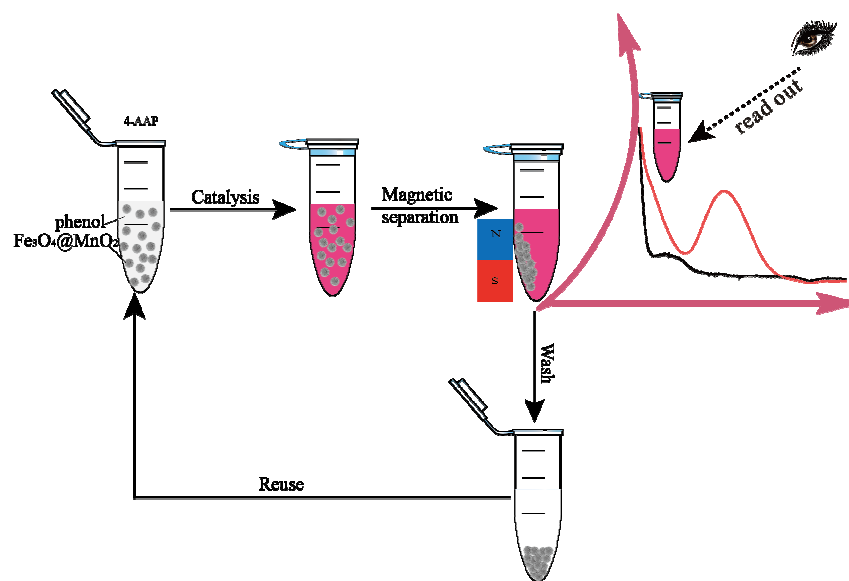
Acknowledgements

Notes and references

[a] *Key Laboratory for the Chemistry and Molecular Engineering of Medicinal Resources (Ministry of Education of China), College of Chemistry and Pharmaceutical Science of Guangxi Normal University, Guilin 541004, P. R. China.*

5 *Corresponding author: Prof. Fanggui Ye*
  Tel: +86-773-5856104; fax: +86-773-5832294
  E-mail address: fangguiye@163.com

1. R. S. Freire, N. Durán and L. T. Kubota, J Brazil Chem Soc, 2002, 13, 456-462.
2. Y. Zhou, L. Tang, G. Zeng, J. Chen, Y. Cai, Y. Zhang, G. Yang, Y. Liu, C. Zhang and W. Tang, Biosensors and Bioelectronics, 2014, 61, 519-525.
3. C. Hu, B. Chen, M. He and B. Hu, J Chromatogr A, 2013, 1300, 165-172.
4. S. Wu, B. Yang, L. Xi and Y. Zhu, J Chromatogr A, 2012, 1229, 288-292.
5. A. Es-haghi, M. Baghernejad and H. Bagheri, Anal Chim Acta, 2012, 742, 17-21.
6. H. Beitollahi, S. Tajik and P. Biparva, Measurement, 2014, 56, 170-177.
7. X. Zhou, L. Liu, X. Bai and H. Shi, Sensors and Actuators B: Chemical, 2013, 181, 661-667.
8. T. Spătaru and N. Spătaru, J Hazard Mater, 2010, 180, 777-780.
9. Y. Zhou, L. Tang, G. Zeng, J. Chen, Y. Cai, Y. Zhang, G. Yang, Y. Liu, C. Zhang and W. Tang, Biosensors and Bioelectronics, 2014, 61, 519-525.
10. J. Ballesta-Claver, M. C. Valencia and L. F. Capitán-Vallvey, Luminescence, 2011, 26, 44-53.
11. Y. He, IEEE, Editon edn., 2011, vol. 2, pp. 1905-1907.
12. R. Sun, Y. Wang, Y. Ni and S. Kokot, J Hazard Mater, 2014, 266, 60-67.
13. R. Sun, Y. Wang, Y. Ni and S. Kokot, Talanta, 2014, 125, 341-346.
14. E. Emerson, J. Org. Chem., 1943, 8, 417-428.
15. M. Ettinger, C. Ruchhoft and R. Lishka, Anal Chem, 1951, 23, 1783-1788.
16. P. Anekthirakun, M. Sukwattanasinitt, T. Tuntulani and A. Imyim, Spectrochimica Acta Part A: Molecular and Biomolecular Spectroscopy, 2013, 111, 91-96.
17. Z. Chen, X. Zhang, H. Cao and Y. Huang, The Analyst, 2013, 138, 2343.
18. J. Gong, D. Li, J. Huang, L. Ding, Y. Tong, K. Li and C. Zhang, Catal Lett, 2014, 144, 487-497.
19. D. Li, S. Ge, J. Huang, J. Gong, T. Wang, P. Yan, G. Li and L. Ding, Sep Purif Technol, 2014, 125, 216-222.
20. R. R. Carballo, V. C. Orto and I. N. Rezzano, Journal of Molecular Catalysis A: Chemical, 2008, 280, 156-163.
21. B. Tang, G. Zhang, Y. Liu and F. Han, Anal Chim Acta, 2002, 459, 83-91.
22. L. Zhu, L. Gong, Y. Zhang, R. Wang, J. Ge, Z. Liu and R. N. Zare, Chemistry - An Asian Journal, 2013, 8, 2358-2360.
23. Z. Lin, Y. Xiao, Y. Yin, W. Hu, W. Liu and H. Yang, ACS Applied Materials & Interfaces, 2014, 6, 10775-10782.
24. D. A. Oriero, J. M. F. Jabal, L. Deobald, A. T. Weakley and D. E. Aston, Reactive and Functional Polymers, 2011, 71, 870-880.
25. J. Xie, X. Zhang, H. Wang, H. Zheng, Y. Huang and J. Xie, TrAC Trends in Analytical Chemistry, 2012, 39, 114-129.
26. Y. J. Long, Y. F. Li, Y. Liu, J. J. Zheng, J. Tang and C. Z. Huang, *Chem Commun*, 2011, **47**, 11939.
27. N. Rajendiran and J. Santhanalakshmi, Journal of Molecular Catalysis A: Chemical, 2006, 245, 185-191.
28. D. Li, S. Ge, J. Huang, J. Gong, P. Yan, W. Lu, G. Tiana and L. Ding, Catalysis Communications, 2014, 45, 95-99.
29. D. Li, Y. Tong, J. Huang, L. Ding, Y. Zhong, D. Zeng and P. Yan, Journal of Molecular Catalysis A: Chemical, 2011, 345, 108-116.
30. K. Yang, M. Zeng, X. Hu, B. Guo and J. Zhou, The Analyst, 2014, 139, 4445.
31. J. Wu, Q. Wang, A. Umar, S. Sun, L. Huang, J. Wang and Y. Gao, New J Chem, 2014, 38, 4420.
32. W. Lai, J. Zhuang, X. Que, L. Fu and D. Tang, Biomaterials Science, 2014, 2, 1073.
33. R. Deng, X. Xie, M. Vendrell, Y. Chang and X. Liu, J Am Chem Soc, 2011, 133, 20168-20171.
34. X. Liu, Q. Wang, Y. Zhang, L. Zhang, Y. Su and Y. Lv, New J Chem, 2013, 37, 2174.
35. X. Liu, Q. Wang, H. Zhao, L. Zhang, Y. Su and Y. Lv, Analyst, 2012, 137, 4552.
36. J. Yan, E. Khoo, A. Sumboja and P. S. Lee, ACS Nano, 2010, 4, 4247-4255.
37. H. Deng, X. Li, Q. Peng, X. Wang, J. Chen and Y. Li, Angewandte Chemie International Edition, 2005, 44, 2782-2785.
38. E. Kim, C. Lee, Y. Chang and Y. Chang, ACS Applied Materials & Interfaces, 2013, 5, 9628-9634.
39. L. Guo, Y. Xu, A. R. Ferhan, G. Chen and D. Kim, J Am Chem Soc, 2013, 135, 12338-12345.
40. L. Zhang, J. Lian, L. Wu, Z. Duan, J. Jiang and L. Zhao, Langmuir, 2014, 30, 7006-7013.
41. W. Qin, L. Su, C. Yang, Y. Ma, H. Zhang and X. Chen, J Agr Food Chem, 2014, 62, 5827-5834.

Graphical Abstract